AIAA JOURNAL
Vol. 41, No. 11, November 2003

Comparison of Experimental and Numerical Studies of Ionizing Flow over a Cylinder

Timothy J. McIntyre,* Alexis I. Bishop,† and Halina Rubinsztein-Dunlop‡
University of Queensland, Brisbane, Queensland 4072, Australia
and
Peter A. Gnoffo§
NASA Langley Research Center, Hampton, Virginia 23681-0001

Comparisons are made between experimental measurements and numerical simulations of ionizing flows generated in a superorbital facility. Nitrogen, with a freestream velocity of around 10 km/s, was passed over a cylindrical model, and images were recorded using two-wavelength holographic interferometry. The resulting density, electron concentration, and temperature maps were compared with numerical simulations from the Langley Research Center aerothermodynamic upwind relaxation algorithm. The results showed generally good agreement in shock location and density distributions. Some discrepancies were observed for the electron concentration, possibly, because simulations were of a two-dimensional flow, whereas the experiments were likely to have small three-dimensional effects.

I. Introduction

THE combined approach of ground-based testing, numerical simulation, and flight testing has advanced greatly in the understanding of complex flows related to supersonic flight. Shock-tunnel testing has provided reliable data up to orbital entry speeds in the vicinity of 8 km/s for comparison with simulations. At these conditions, vibrational excitation and dissociation form the main nonequilibrium chemical processes. At higher (superorbital) speeds, spacecraft entering a planetary atmosphere generate a high-temperature reacting gas flow, which, in many cases, includes appreciable ionization. The electrons have a high mobility, and their rate of generation can have an effect on the pressure distribution and heat loading on the body. The chemistry occurring in the flow involves a large number of reactions, many of which have unknown or uncertain rate coefficients. A lack of experimental data at these conditions means that there are few opportunities for calibration of numerical simulations of such flows.

Superorbital expansion tubes are facilities designed to generate flows with velocities above 10 km/s at densities sufficient to generate thermal and chemical nonequilibrium.[1] They are capable of simulating atmospheric reentry conditions at high speeds, including the presence of ionization. Reentry flows have typically been produced using reflected shock tunnels, where the test gas is accelerated via a steady expansion through a supersonic nozzle. Superorbital facilities can generate flows with higher speeds because the gas is accelerated via an unsteady expansion. Because the gas does not need to pass through a stagnation region at the entrance of a nozzle, enthalpy limiting radiation losses are overcome. The higher speeds are achieved at the cost of shorter test times and smaller core flows. The University of Queensland has developed a number of superorbital facilities ranging from the pilot X1 facility up to the large scale X3 tunnel with an exit diameter of 180 mm.

Received 23 April 2002; revision received 3 May 2003; accepted for publication 19 June 2003. Copyright © 2003 by the American Institute of Aeronautics and Astronautics, Inc. All rights reserved. Copies of this paper may be made for personal or internal use, on condition that the copier pay the $10.00 per-copy fee to the Copyright Clearance Center, Inc., 222 Rosewood Drive, Danvers, MA 01923; include the code 0001-1452/03 $10.00 in correspondence with the CCC.

*Senior Research Fellow, Centre for Hypersonics, Department of Physics.
†Postgraduate Student, Centre for Hypersonics, Department of Physics.
‡Professor, Centre for Hypersonics, Department of Physics.
§Aerospace Engineer, Aerodynamics, Aerothermodynamics, and Acoustics Competency. Associate Fellow AIAA.

This paper reports on a comparison of numerical simulations with previously reported studies of ionizing flows in the midrange X2 facility.[2] In the experiments, nitrogen with a velocity of 10.3 km/s was passed over a cylinder, with the resulting flow imaged using two-wavelength holographic interferometry. This yielded two-dimensional measurements of the density and electron concentration distributions. In regions of chemical equilibrium, it was also possible to extract a flow temperature. The results are compared with numerical simulations generated by the NASA Langley Research Center aerothermodynamic upwind relaxation algorithm (LAURA) code.

II. Experimental Facility

The experiments were conducted in the superorbital expansion tube X2. The facility consists of a driver section, shock tube, and accelerator tube, all separated by diaphragms. A compound piston is used to compress a helium driver gas, causing the bursting of a steel diaphragm. The resulting shock wave passes through the test gas, heating and compressing it. The test gas then ruptures a light plastic diaphragm and expands unsteadily along the acceleration tube to the test section. The gas emerges from the end of the tube and enters the test section and dump tank. The model is mounted at the end of the tube so that it is placed in the core flow. The exit diameter is 85 mm, of which the core flow fills a diameter of about 60 mm, as determined by pitot measurements and numerical simulations.[3] The duration of the test time is approximately 30 μs starting about 10 μs after flow enters the test section.

The comparisons presented here focus on a single superorbital condition with a total enthalpy of 64 MJ/kg, corresponding to an equivalent flight speed of 11.3 km/s. The freestream conditions in the facility were determined through measurements of shock speeds and fill pressures in both the shock and expansion tubes. A computer simulation[3] including viscous effects but assuming chemical equilibrium was used to calculate the conditions at the end of the accelerator tube. These values are shown in Table 1. Static and pitot pressures provided by the code compared favorably with measured values in the facility (static pressure 1.3 ± 0.2 kPa and pitot pressure 170 ± 20 kPa). The density, temperature, and velocity were used as input to the numerical simulations.

The flows were imaged using two-wavelength holographic interferometry.[4] A Nd:YAG laser was used to generate a light beam consisting of 355 and 532 nm components formed to propagate collinearly. The beam was divided into two separate paths, the recording and test beams, each containing both wavelengths. The recording beam was passed above the tunnel using periscopes and then expanded to illuminate the holographic plate. The test beam was

Table 1 Calculated freestream conditions

Parameter	Value
Density	0.0014 kg/m^3
Temperature	3030 K
Velocity	10.3 km/s
Equivalent flight speed	11.3 km/s
Mach number	9.6
Enthalpy	64 MJ/kg
Pressure	1.3 kPa
Pitot pressure	165 kPa

expanded to fill the test section windows and pass over the model. Lenses were then used to image the model onto the holographic plate. An aperture was used at the focus of the beam to remove flow luminosity, particularly in the high-temperature region in front of the body. The recording and test beams reached the plate at an angle chosen for a holographic recording with approximately 2000 lines/mm. To perform interferometry, it was necessary to record no-flow and with-flow holograms. To achieve this, the laser was triggered once before tunnel operation and once during the test time. This created four holograms, which, when reconstructed, generated two independent interferograms, corresponding to the two wavelengths. The interferograms were separately processed to yield phase distributions, which were combined to determine the density and electron concentration.

Under the assumption of chemical and thermal equilibrium, the density and electron concentration are linked by the Saha equation

$$N_e N_I / N_a = \left[2(2\pi mkT)^{\frac{3}{2}} / h^3\right][Q_I(T)/Q_a(T)] \exp(-\chi/kT) \tag{1}$$

where N is the number density, Q is the partition function, χ is the ionization energy, T is the temperature, m is the mass of the species, k is Boltzmann's constant, and h is Planck's constant. Subscripts a refer to the atom, I the ion, and e the electron. All of these parameters are known or measured, apart from T, which can, thus, be extracted by a numerical solution of Eq. (1).[5]

Comparisons between experiment and simulations were performed of flows over cylinders of length 60 mm, one with a diameter of 15 mm and the other 30 mm. The smaller diameter cylinder has a better aspect ratio (length-to-diameter) for generating quasi-two-dimensional flows. However, the larger cylinder provides a bigger shock standoff distance and, hence, more time for chemical equilibrium to be attained. Cylinders were preferred over axisymmetric bodies due to the simpler image analysis to obtain quantitative results. Numerical simulations were performed only for two-dimensional flows, and thus, cylinder end effects were disregarded.

III. Numerical Simulations

The LAURA code[6] was used to simulate the flow. This code employs both a point- and line-implicit relaxation algorithm for solving the viscous hypersonic flow equations, allowing for thermal and chemical nonequilibrium. It uses the two-temperature Park model to allow for separate heavy particle and electron temperatures. It assumes that the translational/rotational energy content of all particles can be described by a distribution based on a single, heavy particle temperature T. In like manner, the vibrational and electronic energy content of all particles is described by a distribution based on a single temperature T_V.

As input, the code used the freestream conditions given in Table 1, assuming a fully two-dimensional cylinder. The wall was assumed to be at room temperature and fully catalytic. Simulations of the tunnel operation[3] show that the freestream was in chemical equilibrium so that there was a corresponding low level of nitrogen dissociation. However, several different freestream dissociation levels c were investigated using the numerical simulation to determine sensitivity of measured data to uncertainties. Implicit in this variation is an associated variation in freestream energy content through the heat of formation of atomic nitrogen. Corresponding sensitivity studies on freestream vibrational/electronic energy levels and energy exchange cross sections are planned. These sensitivity studies establish elements of the physical models in LAURA that are amenable to consistency checks with experimental data. They also aid in interpretation of experimental results.

All solutions were run over a half-cylinder discretized with 40 equally spaced cells in the circumferential direction and 64 cells in the normal direction adapted to the boundary-layer profile and bow shock location. (Faceting of the earliest numerical results for $c = 0.1$ for the 15-mm-diam cylinder arises from plotting options using a subset of the complete solution.) The adaptation algorithm is defined in Sec. 11.1.1 in the LAURA user's manual.[7] Typical grids had cell Reynolds numbers at the surface $(\rho a \Delta n/\mu)_{\text{wall}} < 3$ and maximum grid stretching across the shock layer, $\Delta n_{k+1}/\Delta n_k < 1.2$. Experience with LAURA indicates that these metrics yield grid-converged solutions. An additional check of grid convergence was executed using a grid with double the cells (128) in the normal direction for the 30-mm-diam test case. Sensitive quantities such as heat transfer and temperature distribution across the shock essentially overplotted over most of the stagnation streamline with less than 0.03% difference between the solutions on the two grids. Peak rotational temperature was approximately 6% greater on the finer grid. The overshoot region of rotational temperature across the shock front was resolved with 13 cells on the nominal grid and 23 cells on the finest grid. The shock front steepened slightly on the finest grid, though total shock standoff distance changed less than 2%; consequently, numerical viscosity is not indicated as a substantial contributor to dissipation across the shock front. Grid clustering at the shock front is engaged in these comparisons.

All solutions were converged using implicit line relaxation to order 10^{-8} or less as measured by the L_2 norm of all residuals. Computational times for the nominal grid on an SGI Octane, single CPU, are less than 30 min from a cold start initialized with freestream conditions.

A fully catalytic wall boundary condition was specified forcing mass fractions of atoms and ions to trace amounts at the wall. This condition is the most stable numerically and is a reasonable representation of a clean, metallic surface. This boundary condition has negligible consequence on the current set of measurements, but can significantly impact[8] levels of surface heating if atoms are present at the boundary-layer edge and chemical nonequilibrium persists across the boundary layer.

Lee[9] and Park[10] have discussed justifications and limitations of the empirical two-temperature model used herein. The assumption is based on knowledge of rapid energy exchange between electron translational mode and molecular vibrational modes.

IV. Results and Discussion

Interferograms of the flow over the 15- and 30-mm-diam cylinders are reproduced in Fig. 1.[2] For the 15-mm-diam cylinder, the image is recorded about 10 μs into the test time, whereas for the 30-mm-diam cylinder, the image was recorded about 20 μs into the test time. The images show a sharp jump in the fringes defining the location of the shock wave. For the 532-nm interferograms, the fringes behind the shock front show a slight reversal in direction, indicating the formation of electrons. Close to the model, a further fringe shift is observed where the presence of the body is affecting the flow.

The interferograms were analyzed to yield two-dimensional distributions of the flow parameters[4,5] for comparison with the simulations. This was performed at two levels of resolution. The full field was analyzed using 1024×1024 pixels to show the general features of the flow. Because this only utilizes a relatively small number of pixels between the shock and the body, a higher resolution analysis was also performed. This focused on the region in the vicinity of the stagnation streamline between the shock and the body. The latter analysis was used to generate the experimental data along the stagnation line, whereas the former was used for two-dimensional comparisons.

The initial comparisons examined the conditions along the stagnation streamline for the 15-mm-diam cylinder. Figure 2 shows values for the density and electron number density from the experiments and the simulations along the stagnation streamline. Uncertainties

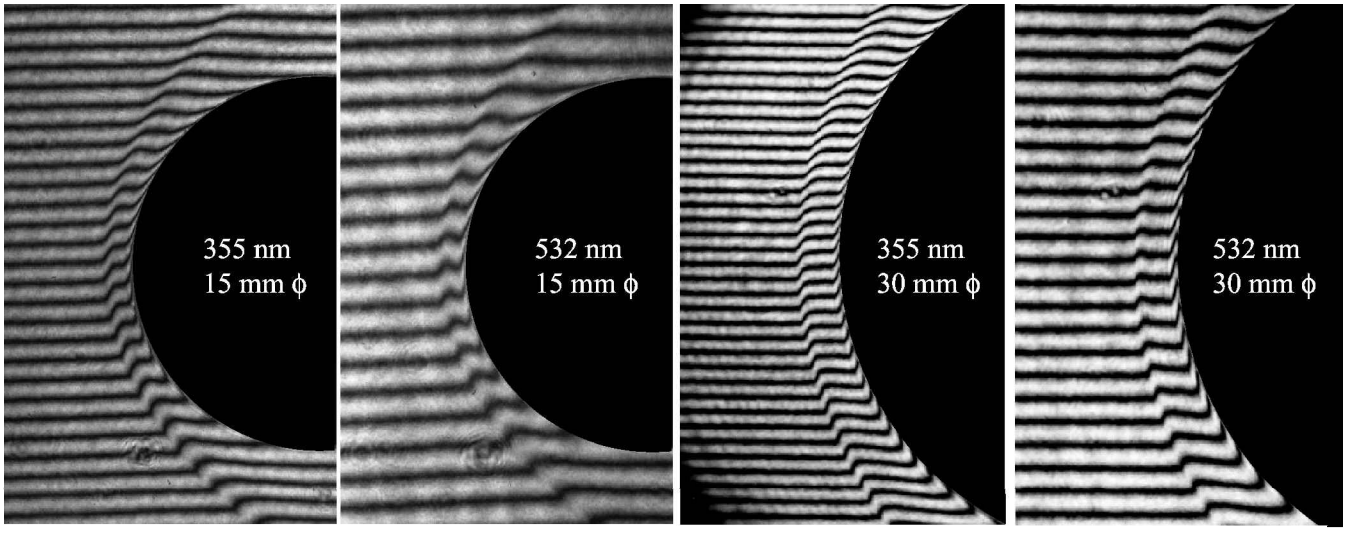

Fig. 1 Holographic interferograms of flow over 15- and 30-mm-diam cylinders; flow left to right.

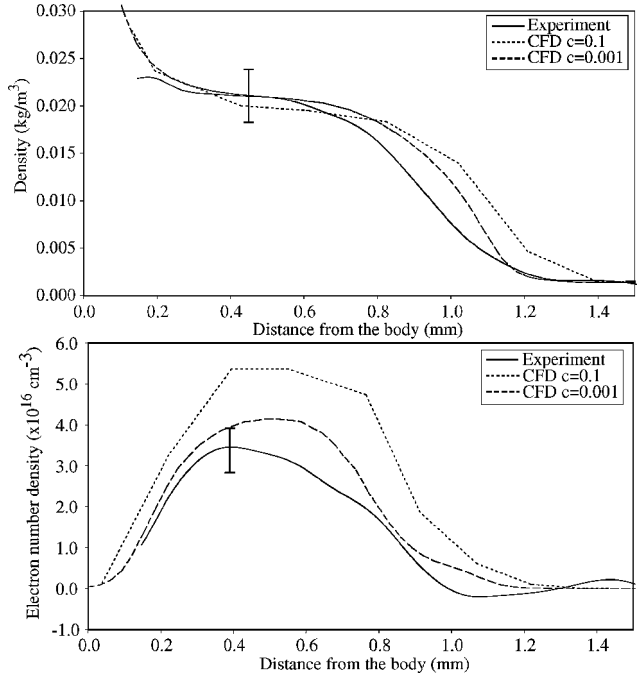

Fig. 2 Comparison of experimental measurements and numerical simulations [computational fluid dyncamics (CFD)] along the stagnation streamline for the 15-mm-diam cylinder.

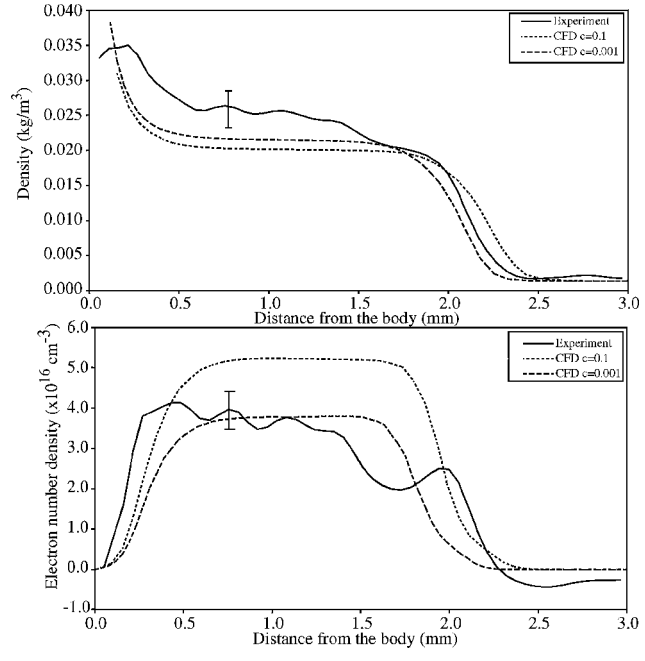

Fig. 3 Comparison of experimental measurements and numerical simulations (CFD) along the stagnation streamline for the 30-mm-diam cylinder.

in the experimental values are due to the accuracy of the phase retrieval system and due to the unknown refractivity of the nitrogen ions. A quantity that is not directly measured in the experiments is the freestream dissociation level c. Because the facility generates the high speeds by heating the test gas and then allowing it to expand, it is possible that the nitrogen molecules may be dissociated and are unable to recombine due to chemical freezing in the expansion process. This results in a higher dissociation level in the freestream than would be otherwise expected if the flow was in chemical equilibrium. Figure 2 shows simulated densities for a moderate dissociation level ($c = 0.1$) and a low level of dissociation ($c = 0.001$). A higher dissociation level in the freestream results in a larger shock standoff distance and a higher peak electron concentration. Figure 2 shows that there is a good agreement between the experiment and the simulation using the lower dissociation. This is consistent with the numerical simulations of the tunnel operation that calculate that the freestream is in chemical equilibrium and, thus, has a very low dissociation level. The comparisons for the flow density show that there is reasonable agreement for the location of the shock wave and good agreement for the level where the density reaches a plateau. Interestingly, neither trace shows a sharp increase in density across the shock front, despite there being good resolution in both the experiment and the simulation. One possible explanation for a smearing of the shock front in the experimental measurements is the finite length of the cylinder. For the traces in Fig. 2, the cylinder has an aspect ratio (length-to-diameter) of four, and thus, three-dimensional effects may be important. However, the numerical simulations cover only a two-dimensional case and, thus, do not have any edge effects included. The results for the electron concentration also show good agreement for the lower dissociation level calculation. Both show that the liberation of electrons is delayed somewhat behind the shock front. A sharp rise is observed at about 0.8 mm from the cylinder compared to the shock location at about 1.1 mm. Neither experiment nor simulation show a plateau in the electron concentration, indicating that chemical equilibrium is not reached between the shock front and the body. The influence of the body results in a sharp drop in the electron concentration at about 0.4 mm from the surface.

The results for measured parameters for the 30-mm-diam cylinder along the stagnation are shown in Fig. 3. The larger diameter

generates a larger shock standoff distance of about 2.2 mm. In this case, the agreement between the numerical and experimental values is also good, particularly for the level of ionization. One possible source of discrepancy lies in the dimensions of the cylinder used in this case. Here the body has an aspect ratio of only two. The assumption of a two-dimensional flow, as used in the image analysis, is then questionable. In reality the bow shock will be curved in front of the body, reducing the optical pathlength and generating varying gas conditions along the line of sight of the optical system. The effect will be more pronounced nearer the shock, where the curvature has a more significant effect. This conclusion is consistent with the observation in Fig. 3 that both the experimentally measured density and electron concentration continue to rise slowly behind the shock front. In contrast, the numerical simulations show that there is sufficient time for the flow to attain chemical equilibrium as seen by the plateau.

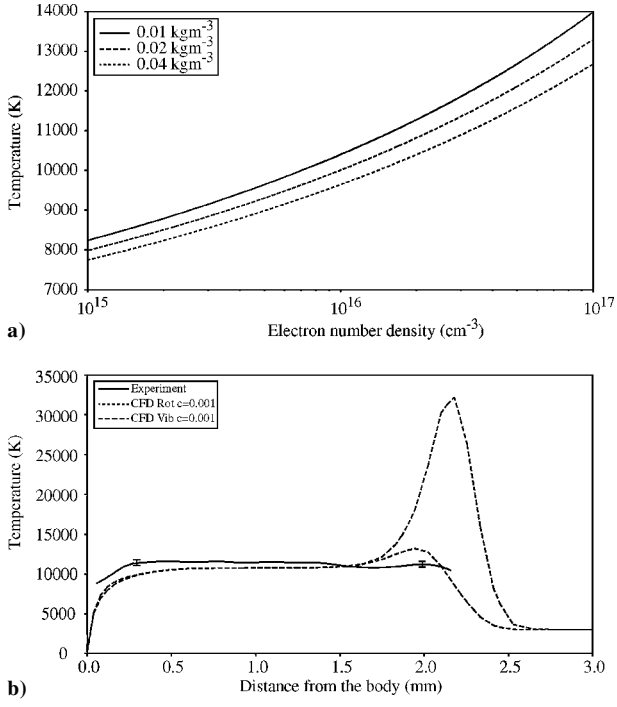

Fig. 4 Determination of temperature where Rot is rotational/translational and Vib is vibrational/electronic temperature: a) dependence of temperature on electron concentration and b) comparison of experimental measurements and numerical simulations (CFD) of temperature along the stagnation streamline for the 30-mm-diam cylinder.

The observed equilibrium region for the larger cylinder provides a region where temperature can be inferred from the measurements. As discussed, temperatures determined in this manner are valid only in regions of chemical equilibrium containing measurable quantities of electrons. The results indicate that equilibrium is not established behind the bow shock for the 15-mm-diam cylinder, and hence, it is not valid to determine a temperature. For the 30-mm-diam cylinder, however, simulations and measurements would indicate that equilibrium is established in the vicinity of the stagnation streamline behind the bow shock. Equation (1) is used to determine the temperature based on the measured density and electron concentration. To illustrate the sensitivity of this method to varying flow conditions, Fig. 4a shows the calculated temperature as a function of electron number density for several values of the total density. An order of magnitude change in the electron concentration leads to a temperature change of several thousand Kelvin.

Figure 4b shows the application of Eq. (1) to the data shown in Fig. 3 to obtain an experimental flow temperature along the stagnation streamline. Simulated values are provided for both the translational temperature and the vibrational temperature. Because the measured temperature is determined by examining the electron concentration compared to the total density, it is correct to interpret the experimental temperature as the vibrational temperature, assumed equal to the electron temperature. Note that this temperature measurement is less sensitive to the optical pathlength because it is calculated from a ratio of density values both dependent on the length of the model. This length then divides out of the resulting equation, and the finite length of the cylinder is only important through any variations in conditions along the laser beam. Uncertainties in the experimental measurement are based on the uncertainties for the density and electron concentration measurements. Because of the logarithmic relationship between the temperature and the species

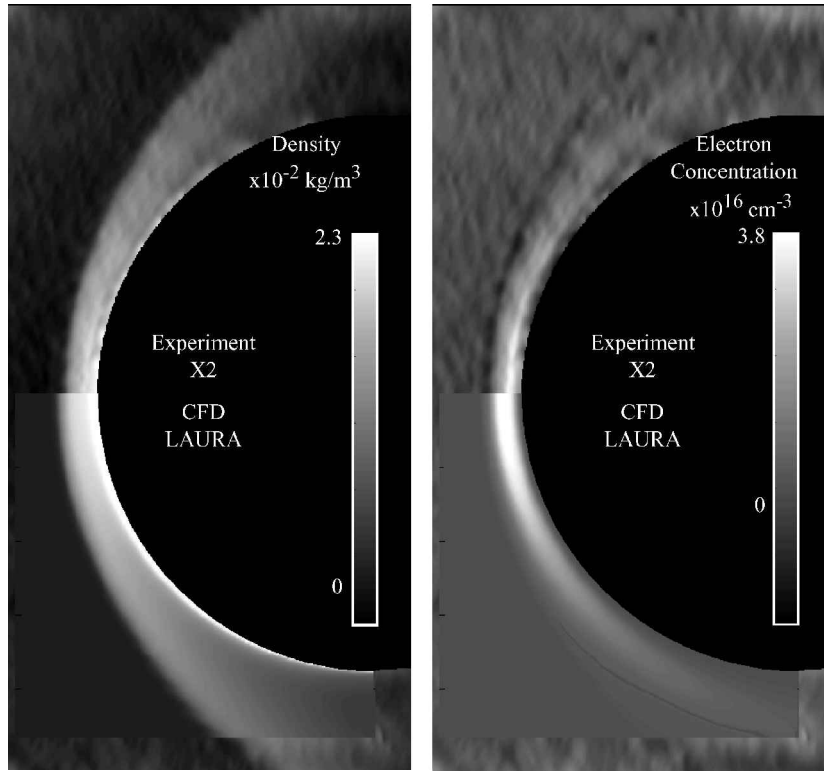

Fig. 5 Comparison of experimental measurements and numerical simulations for the 15-mm-diam cylinder; flow left to right.

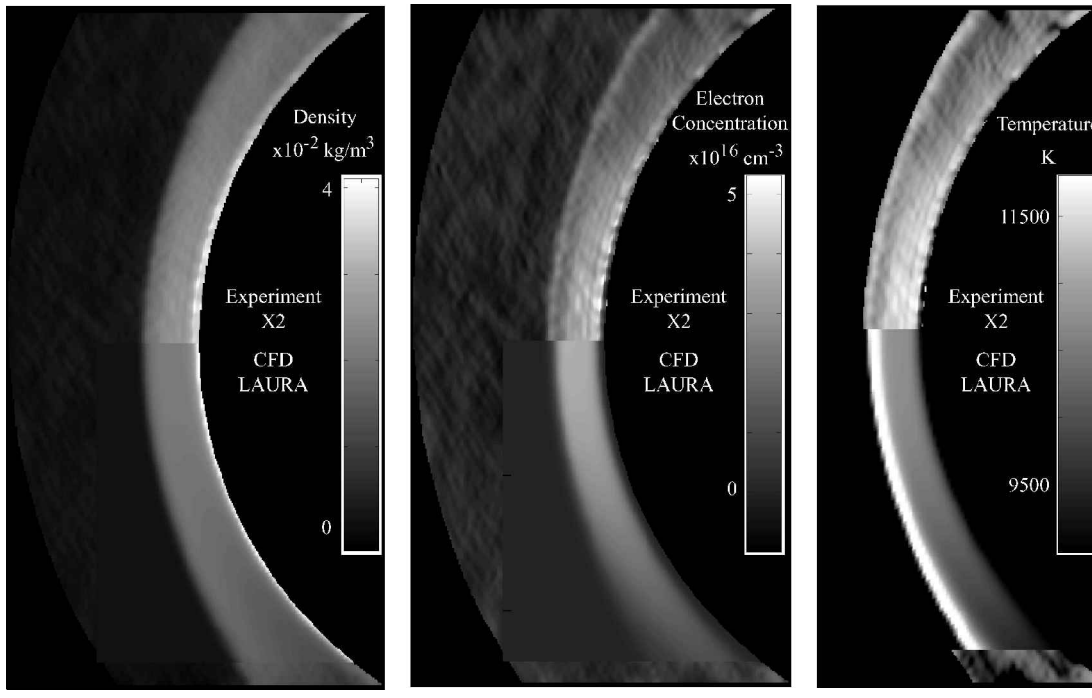

Fig. 6 Comparison of experimental measurements and numerical simulations for the 30-mm-diam cylinder; flow left to right.

concentration, the relative error in the temperature measurement is significantly smaller than the values for density and electron concentration. Figure 4b shows that the translational/rotational temperature initially rises to a high level due to shock compression. The vibrational/electron temperature is initially lower because electrons generated at this stage have a relatively small kinetic energy. As energy is transferred between the heavy particles and electrons, the temperatures converge. At equilibrium, the measured temperature and the simulated temperatures show reasonable agreement, although the simulated value falls below the measured value nearer the body.

Experimental measurements in two dimensions from the lower resolution analysis are shown in Figs. 5 and 6. Figure 5 shows density and electron concentrations throughout the flow for the 15-mm-diam cylinder. Overlaid on Fig. 5 are the numerical simulations for this cylinder, where it was assumed that the freestream dissociation level was 0.001. In general, the agreement between experiment and theory appears good. Both experiment and simulation show similar trends near the model, an increase in density and decrease in electron concentration. The extent of the region in which electrons are liberated is similar in each case. The shock standoff is slightly larger for the simulations, although the experimentally measured distance contains an uncertainty of about 0.1 mm due to the difficulty of precisely identifying the model position in the lower resolution image. Figure 6 shows the corresponding results for the 30-mm-diam cylinder. The differences between experiment and simulation observed along the stagnation streamline for the larger cylinder are also reflected in other parts of the flow.

V. Conclusions

Comparisons have been made between experimental and numerical studies of flows in a superorbital expansion tube. The results show generally good agreement for the shock standoff distance, the density distribution, the electron concentration, and, where measured, the temperature. For the 15-mm-diam cylinder, it was found that there was insufficient time for the flow passing through the bow shock to attain chemical equilibrium. In contrast, the 30-mm-diam cylinder generated a larger shock standoff and, hence, larger residence time allowing an equilibrium state to be reached. However, the experimental results indicated that the larger cylinder was not sufficiently long to generate a quasi-two-dimensional flow; some differences were observed between calculation and experiment.

Acknowledgments

This work has been partially funded through grants from the Australian Research Council. The authors thank Richard Morgan for his assistance with the experiments. The input of the Mechanical Workshops of the Departments of Physics and Mechanical Engineering is gratefully acknowledged.

References

[1]Neely, A. J., and Morgan, R. G., "The Superorbital Expansion Tube Concept, Experiment and Analysis," *Aeronautical Journal*, Vol. 98, No. 973, 1994, pp. 97–105.

[2]McIntyre, T. J., Bishop, A. I., Thomas, A. M., Sasoh, A., and Rubinsztein-Dunlop, H., "Ionizing Nitrogen and Air Flows in a Superorbital Expansion Tube," *AIAA Journal*, Vol. 38, No. 9, 2000, pp. 1685–1691.

[3]McIntyre, T. J., Jacobs, P. A., Bishop, A. I., and Boyce, R. R., "Experimental and Numerical Studies of Super-Orbital Ionising Flows," *Proceedings of the 22nd International Symposium on Shock Waves*, edited by G. J. Ball, R. Miller, and G. T. Roberts, Univ. of Southampton, Southampton, England, U.K., 2000, Paper 1350.

[4]McIntyre, T. J., Wegener, M. J., Bishop, A. I., and Rubinsztein-Dunlop, H., "Simultaneous Two-Wavelength Holographic Interferometry in a Superorbital Expansion Tube Facility," *Applied Optics*, Vol. 36, No. 31, 1997, pp. 8128–8134.

[5]McIntyre, T. J., Bishop, A. I., and Rubinsztein-Dunlop, H., "Two-Wavelength Holographic Interferometry as a Diagnostic Tool for Ionising Flows," *Proceedings of the Millennium 9th International Symposium on Flow Visualization*, edited by G. I. Carlomagno, Edinburgh, 2000.

[6]Gnoffo, P. A., "Upwind-Biased, Point-Implicit Relaxation Strategies for Viscous, Hypersonic Flows," AIAA Paper 89-1972, Jan. 1989.

[7]Cheatwood, F. M., and Gnoffo, P. A., "User's Manual for the Langley Aerothermodynamic Upwind Relaxation Algorithm (LAURA)," NASA TM 4674, April 1996.

[8]Gnoffo, P. A., Weilmuenster, K. J., Hamilton, H. H., II, Olynick, D. R., and Venkatapathy, E., "Computational Aerothermodynamic Design Issues for Hypersonic Vehicles," *Journal of Spacecraft and Rockets*, Vol. 36, No. 1, 1999, pp. 21–43.

[9]Lee, J.-H., "Basic Governing Equations for the Flight Regimes of Aeroassisted Orbital Transfer Vehicles," *Thermal Design of Aeroassisted Orbital Transfer Vehicles*, Vol. 96, Progress in Astronautics and Aeronautics, AIAA, New York, 1985, pp. 3–53.

[10]Park, C., "Problems of Rate Chemistry in the Flight Regimes of Aeroassisted Orbital Transfer Vehicles," *Thermal Design of Aeroassisted Orbital Transfer Vehicles*, Vol. 96, Progress in Astronautics and Aeronautics, AIAA, New York, 1985, pp. 511–537.

G. V. Candler
Associate Editor